

## Lecture 9 Solar Radiation Transfer Through Vegetation, Part 2: Theory

Instructor: Dennis Baldocchi  
Professor of Biometeorology  
Ecosystem Science Division  
Department of Environmental Science, Policy and Management  
345 Hilgard Hall  
University of California, Berkeley  
Berkeley, CA 94720

September 26, 2014

### Lecture Topics

1. Scattering Theory
  - a. leaf optical properties
2. Two-Stream Models for Radiative Transfer through Vegetation
3. Modeling Albedo
4. Remote Sensing

### L9.1 Scattering

When leaves **intercept** photons, they either **reflect**, **transmit** or **absorb** them. The sum of the reflected and transmitted light is called **scattering**. Light transmitted through leaves undergo several modes of transfer through its optical path.

The structure of cells in the mesophyll of leaves is large relative to the wavelength of light [*Gates*, 1980; *Gates et al.*, 1965]. Visible light is in the 0.4 to 0.7 micron range. Cells of plants are on the order of 15 by 15 by 60 microns. The grana in the chloroplast are small, 0.05 micron and can scatter light.

Light passing through a leaf will undergo (see Tang, 1999):

- a. **lens effect**: caused by liquids and oils in leaves
- b. **sieve effect**: the heterogeneous distribution of pigments enables light to pass through tissue.
- c. **optical wave guide**: when light is reflected back and forth between two parallel surfaces.
- d. **light trapping**: the refractive index of cuticle (1.45) is greater than air (1.0), so it can reflect exiting photons back inside the leaf. The scattering of light inside a leaf increases its optical path. This phenomenon increases the probability of a photon being absorbed.

The earliest theories on leaf reflection date back to work by Willstater and Stoll (1918), who argued that reflection was due to the reflection of photons at the cell wall- air interface of spongy mesophyll. Modern studies have found that this theory does not account for specular reflection of leaves. Mathematically analyzed by Sinclair, Gaussman, Allen and others show that leaf reflection is a function of the total area of cell wall-air interface, not the volume of air spaces. Therefore, it was found that the palisade parenchyma were also important contributors to scattering.

Factors affecting leaf optical properties include surface roughness, refractive index of cuticle, composition, amount and distribution of pigments, internal leaf structure and distribution of water [Ross, 1980].

Photon energy is absorbed selectively by **plant pigments**, which either convert the energy **to heat**, they **fluoresce** or use the energy for **photosynthesis**. The predominant pigments in leaves are **chlorophyll a and b, alpha and beta carotene** and **xanthophyll**. **Chlorophyll** absorbs in the red, green, Ps1 (700) and Ps2 (680) photoreceptors.

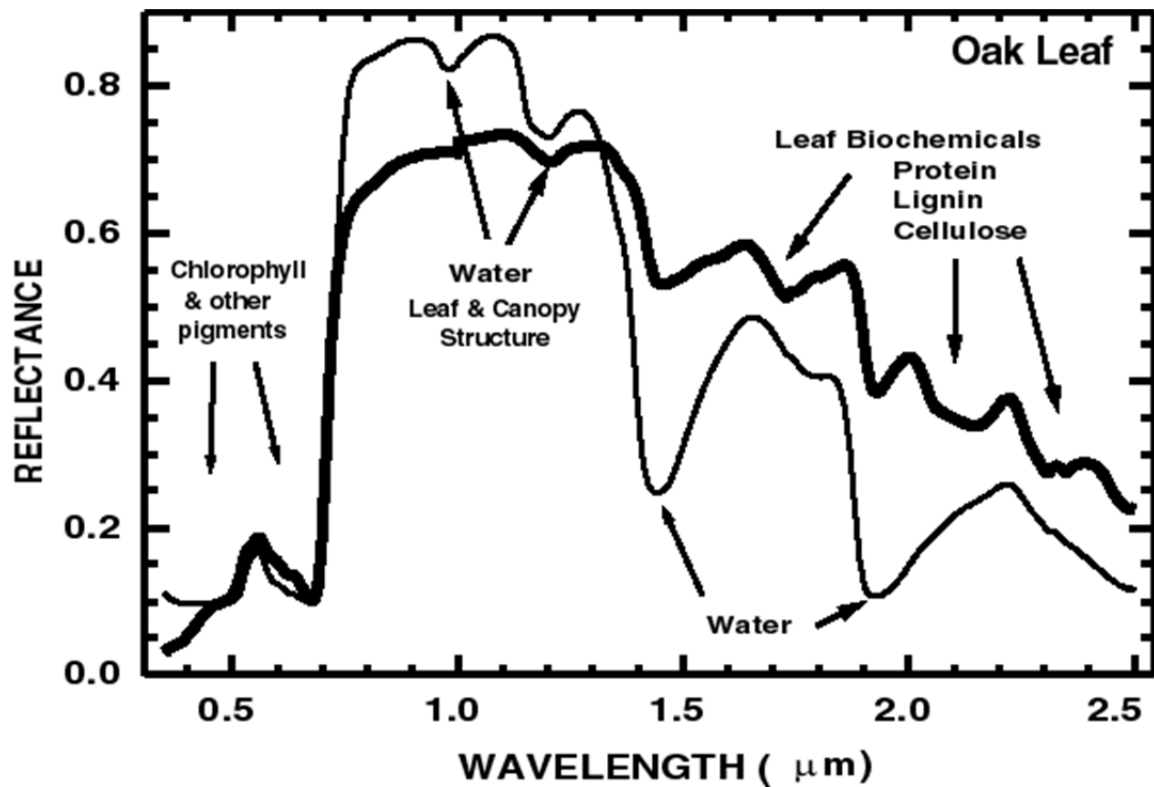


Figure 1 Spectrum of a leaf, data from : [speclab.cr.usgs.gov/national.parks/Yellowstone/jplfig2.gif](http://speclab.cr.usgs.gov/national.parks/Yellowstone/jplfig2.gif)

Optical properties (reflection and transmission coefficients) of leaves are needed to calculate scattering of intercepted radiation [Myneni *et al.*, 1989; Ross, 1980]. Preferred absorption and scattering of selected wavebands act to alter the composition of solar radiation with depth into a canopy (Smith, 1980). Absorption is high (eg. 90%) in the

photosynthetically active waveband, and low (15 to 20%) in the near infrared bands (wavelengths > 0.7 μm).

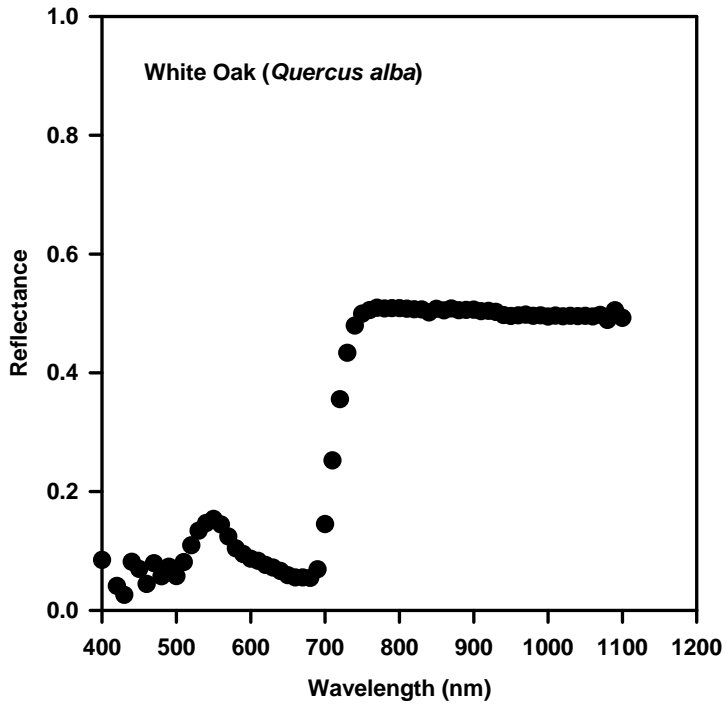


Figure 2 Reflectance spectrum of a white oak leaf

Data for optical reflectance, transmittance and absorption are compiled on a broadband basis are listed in the following table for PAR, NIR and shortwave

Table 1 Typical optical properties for green leaves

	PAR, Visib le	NIR	Solar shortwave
reflectance	0.09	0.51	0.30
transmittance	0.06	0.34	0.20
scattering	0.15	0.85	0.50
absorptance	0.85	0.15	0.50

Again, note how the shortwave reflectance is not the algebraic average of visible and NIR terms!

The angular distribution of light scattered by a canopy is a function of the scattering phase function, integrated over the distribution of leaf normals and the leaf scattering phase function [Myneni *et al.*, 1989; Ross, 1980].

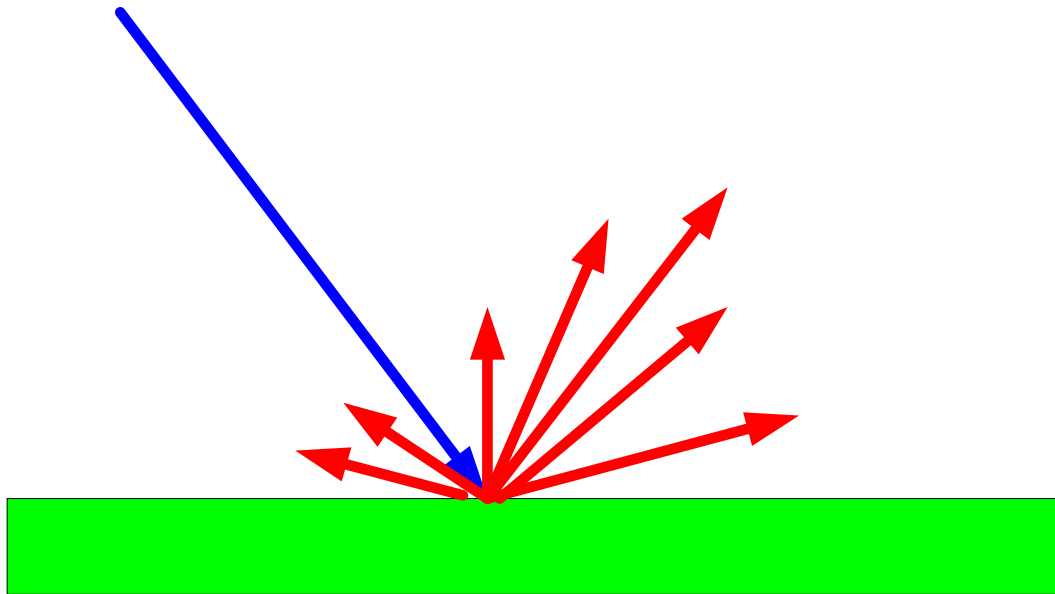


Figure 3 Phase angle distributions of scattered light from leaves

Numerical models are used to model scattering (Bonhomme, Myneni *et al.*, 1989). One approach examines the scattering along solid angle sectors. This approach can deal with varying sky illuminance and directional reflection and transmission. A broader approach divides the canopy into vegetated layers. It treats the upward and downward fluxes for each layer and can consider leaf angle distributions. The **successive orders of scattering** is a method that can account for multiple (higher order scattering, which is important in the NIR). Monte Carlo models are able to simulate three-dimensional arrays of leaves and using statistically, random sampling methods can trace the movement of photons in the canopy.

To compute scattering, a phase function is introduced to describe the angular distribution of scattering. With pure scattering, the probability that light from a given direction leaves a solid from another angle is  $P(\Omega_x, \Omega_y)$ .

$$\frac{1}{4\pi} \int_{\Omega} P(\Omega', \Omega) d\Omega = 1$$

We next introduce the area scattering phase function, the probability that incident radiation in direction  $\Omega'$  is scattered in direction  $\Omega$  can be defined by the single scattering and the probability that the beam is intercepted (G):

$$\frac{1}{\pi} \int_{\Omega} \Gamma(\Omega', \Omega) d\Omega = G_{\Omega'} \omega_s$$

The diffuse component is scattered isotropically and follows Lambert's cosine law.

### L9.2 Modeling Radiative Transfer in Vegetation

The steady-state transport equation for photons transfer is used as a starting point to assess photon transfer through vegetation with flat horizontal leaves [Myneni *et al.*, 1989; Ross, 1980]

$$-\cos \gamma \frac{dI(z, \Omega)}{dz} = -k(z, \Omega)I(z, \Omega) + \frac{1}{\pi} \int_{4\pi} d\Omega' \cdot \omega_s(z, \Omega' \rightarrow \Omega) \cdot I(\tau, \Omega')$$

$\sigma_e$  is the extinction coefficient

$\omega_s$  is the differential scattering coefficient

$I$  is the light flux density and  $k$  is the extinction coefficient

The scattering relates to the transfer of photons coming from  $\Omega'$  and being scattered in a solid unit angle  $\Omega$ .

To apply this equation for plant canopies we must make some transformations .

For photon transport through vegetation the extinction coefficient can be viewed in terms of leaf area density and the orientation of the leaves,  $k(z, \Omega) = G(z, \Omega)a(z)$ . The extinction coefficient relates to the probability per unit length of travel that a photon hits a leaf.  $G$  is the fraction of total leaf area per unit volume of canopy that is perpendicular to a leaf, divided by the travel distance.

This equation assumes no polarization of light and there are not radiation sources along the travel path. Conceptually, this equation represents the various streams of photons

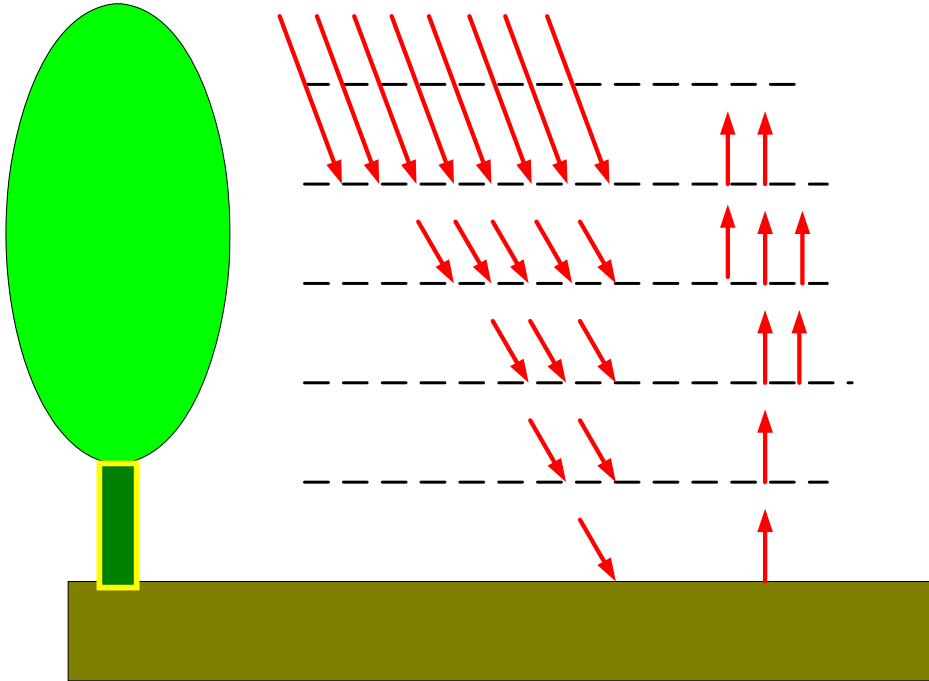


**Figure 4** One dimensional flows of photons in a layered plant canopy. No beam transmission is represented in this figure.

To apply this equation to a plant canopy we have to recognize that the extinction coefficient may vary along the path. Various frames of reference can be used to model radiative transfer through vegetation. Often we use the optical depth ( $\tau$ ), as denoted from cumulative leaf area, starting from the top of the canopy (Myneni et al., 1989, Ross, 1981; Sinoquet et al., 1995).

$$\tau = \int_0^z a(z) dz$$

$$\frac{\cos \theta}{a(z)} \frac{dI}{dz} = \cos \theta \frac{dI}{d\tau}$$

$$-\cos \theta \frac{dI(\tau, \Omega)}{d\tau} = -G(\tau, \Omega) I(\tau, \Omega) + \frac{1}{\pi} \int_{4\pi} d\Omega' \cdot \Gamma(\tau, \Omega': \Omega) \cdot I(\tau, \Omega')$$

In this form the **change in I** across a differential of leaf area  $\tau$  equals the **loss in radiation** due to the **interception** in the direction  $\Omega$  plus the **gain in radiation** in direction  $\Omega$  from radiation of the source direction  $\Omega'$ .

The simplest case, with no scattering and black leaves, reverts back to a form of **Beer's Law**, but in the direction of the beam

$$\frac{dI(\tau, \Omega)}{d\tau} = -\frac{G(\tau, \Omega)}{\cos\theta} I(\tau, \Omega)$$

$$I(\tau, \Omega) = I(0, \Omega) \exp\left(-\frac{G\tau}{\cos\theta}\right)$$

Various cases can be defined with scattering, which reduces or increases the complexity with which it is evaluated. Simple cases include azimuthal symmetry, equal reflectance and transmittance and single isotropic scattering.

For the case of single-scatter albedo, where the reflection is independent of the direction of the incoming and outgoing radiation we have:

$$\int_{4\pi} d\Omega \cdot \Gamma(\tau, \Omega' \rightarrow \Omega) = \varpi$$

If scattering depends on leaf orientation and photon direction then we use:

$$\frac{1}{\pi} \int_{4\pi} d\Omega' \cdot \Gamma(\tau, \Omega' \rightarrow \Omega) = \varpi G(\Omega')$$

Among the earliest attempts to model radiative transfer through turbid media were efforts by Kubelka-Munk [*Kubelka*, 1948; *Kubelka and Munk*, 1931] and Duntley (1942). These models assumed **one dimensional transfer and isotropic scattering** of light. Models based on their ideas are valid for hemispherical radiative transfer, but they are poor representation of non-isotropic scattering and specular reflection.

Nevertheless, such models are adequate for many biometeorological applications such as computing canopy photosynthesis and evaporation. Let's look at the conceptual model of Suits [1971], who modified the Kubelka-Munk equation for photon transfer through vegetation. The first equation describes how downward-directed diffuse radiation,  $I \downarrow$ , varies with changes in optical depth,  $\tau$ :

$$\frac{dI \downarrow}{dx} = -(k + s)I \downarrow + sI \uparrow$$

where  $a$  is an attenuation coefficient,  $b$  is a scattering coefficient, and  $c$  is a coefficient for the conversion of direct into downward-directed diffuse radiation. This equation shows how change in downward directed sunlight is **diminished** by the amount of diffuse radiation that is attenuated by a layer of leaves and it is **augmented** by the amount of upward directed diffuse radiation and beam radiation that are scattered downward. The scattering factors are for layers not leaves.

The second equation represents the change of upward directed diffuse radiation with a change in the optical depth,  $\tau$ :

**Equation 1**

$$\frac{dI^\uparrow}{dx} = (k + s)I^\uparrow - sI^\downarrow$$

This flux density of radiation is *diminished* by the amount of diffuse and beam radiation that is scattered and is **augmented** by the amount of upward directed diffuse radiation that is transmitted through the layer. The scattering coefficients  $a_3$  and  $a_4$  sum to one.

The third equation represents the attenuation of beam radiation by canopy layers (the relation used to form Beer's Law):

**Equation 2**

$$\frac{dI_{beam}}{d\tau} = -k \cdot I_{beam}(\tau)$$

The radiative transfer mode of Norman [Norman, 1979; Norman and Jarvis, 1975; Norman et al., 1971] provides a set of discrete equations for the transmission, interception and reflection of direct and diffuse in discrete wavebands (e.g. visible, near infrared and infrared radiation) through one dimensional canopies. Downward-directed flux density of diffuse light ( $I_D^\downarrow$ ), at layer specific layer in a canopy ( $i$ ) for a given waveband, is defined as the sum of the downward directed diffuse radiation that was transmitted from the upper layer ( $\tau I_D^\downarrow$ ) and the upward directed radiation that is reflected downward ( $\rho I_D^\uparrow$ ):

$$I_D^\downarrow(i) = R \cdot I_D^\uparrow(i) + T \cdot I_D^\downarrow(i+1)$$

**Equation 3**

Similarly, the upward directed diffuse sunlight ( $I_D^\uparrow$ ) is a function of that radiation which is transmitted through the layer and the reflected downward radiation:

$$I_D^\uparrow(i+1) = R \cdot I_D^\downarrow(i+1) + T \cdot I_D^\uparrow(i)$$

**Equation 4**

The transmission and reflectance of sunlight through layers of vegetation ( $\Delta f$ ) are defined as:

$$T_n = \exp\left(\frac{-\Delta f \cdot G \cdot \Omega}{\sin \beta}\right) + \left(1 - \exp\left(\frac{-\Delta f \cdot G \cdot \Omega}{\sin \beta}\right)\right)\tau$$

**Equation 5**

$$R_u = \left(1 - \exp\left(\frac{-\Delta f \cdot G \cdot \Omega}{\sin \beta}\right)\right)\rho_u$$

**Equation 6**

$$R_l = \left(1 - \exp\left(\frac{-\Delta f \cdot G \cdot \Omega}{\sin \beta}\right)\right)\rho_l$$

**Equation 7**

In Equations 32-34,  $\rho$  is the leaf reflectance and  $\tau$  is the leaf transmittance for the specific waveband. The subscripts  $u$  and  $l$  refer to the upper and lower sides of the leaves. We can consider clumping of foliage by including the Markov clumping factor,  $\Omega$ , in the exponential function for light penetration through gaps.

The interception and subsequent scattering of sunlight produces complementary radiation that changes with depth and waveband, as shown in Figure 11 for a forest canopy. The scattering coefficient of PAR is relatively low, so its diffuse radiation decreases with depth in a semi-exponential manner. The scattering of NIR, by contrast is high, over 50%. In the upper quarter of the canopy diffuse NIR increases with depth, then it experiences an exponential decay with further depth.

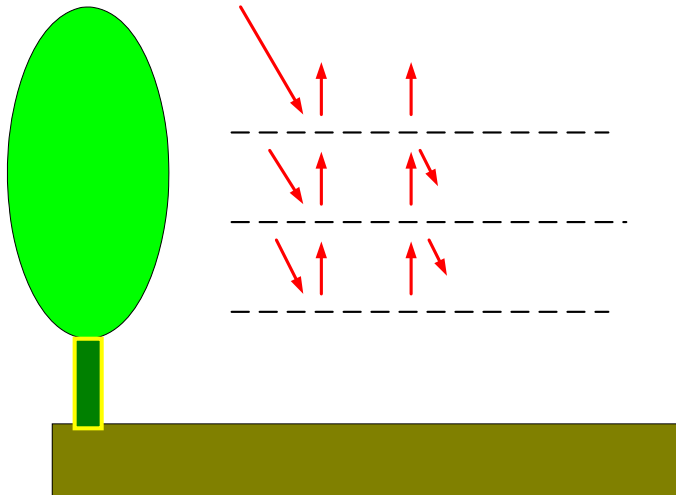


**Figure 5** Flows of photons across adjacent layers. Note the transmission of photons through layers, the upward and downward scattering, the upward transmission of scattered light through gaps and the potential for multiple scattering.

The impact of scattering on producing complementary radiation with depth in a forest canopy is shown below. The scattering coefficient of PAR is relatively low, so its diffuse radiation profile decreases with depth in a semi-exponential manner. The scattering of NIR, by contrast is high, over 50%. In the upper quarter of the canopy diffuse NIR increases with depth, then it experiences an exponential decay with further depth.

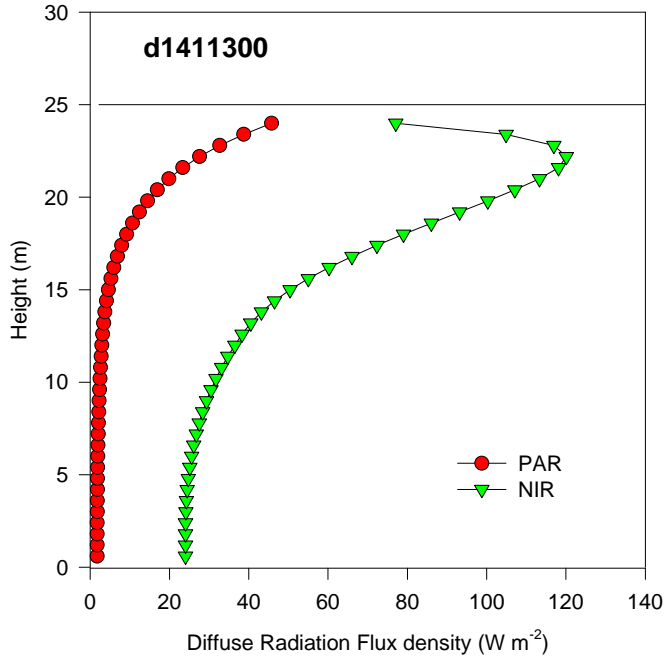


**Figure 6 Profiles of diffuse radiation in the NIR and PAR wavebands**

### L9.3 Modeling Albedo

As a first approximation, one may expect the albedo of a canopy to be close in value to the reflectivity of leaves; this is yet another example of a scale emergent property, e.g. the sum of the individuals don't quite relate to that of the whole. Yet measured albedos of canopies are often half the value of leaves [Dickinson, 1983]. With respect to a broadleaved forest Birkebak and Birkebak (1964) report that the shortwave radiation, scattering coefficient of white oak is 0.52. In contrast, canopy scale albedo measurements are on the order of 0.10 to 0.15 (Hutchison and Baldocchi, 1989). Light trapping by leaves, successively deeper in the canopy, reduce the canopy albedo, relative to leaf reflectances [Dickinson, 1983]. This successive trapping can aid to explain the relationship between albedo and canopy height that is noted in the literature.

The albedo of a canopy is a function of the direction of the incoming source of radiation. If the forward and backward scattering of light by leaves is isotropic then the scattering phase function is independent of solar zenith angle. If we are interested at the albedo at the top of a canopy, where  $L$  equals zero we can assess the algebraic relation for single scattering albedo, at the limit where scattering and leaf area go towards zero [Dickinson, 1983]. For a semi-infinite canopy with horizontal leaves and equal leaf reflectivity and transmissivity, the canopy albedo is:

**Equation 8**

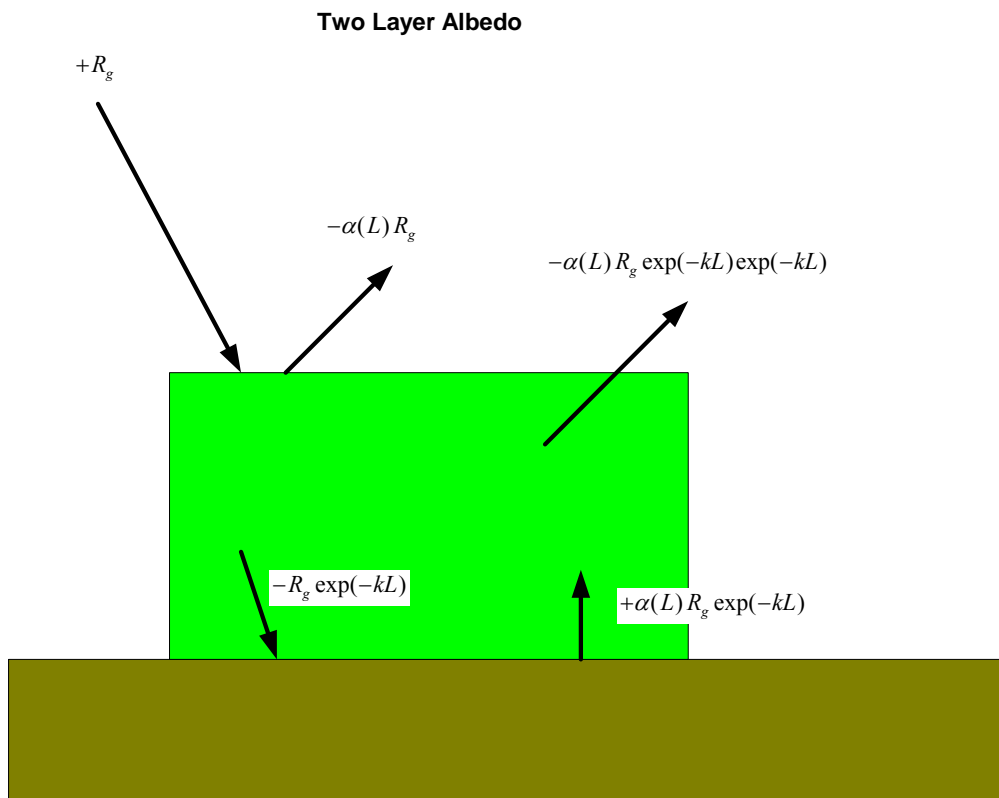
$$\alpha_{canopy} = \frac{\varpi}{(1 + (1 - \varpi)^{1/2})^2}$$

This relation can be derived from the two-stream model of radiative transfer. For single scattering albedo is about one-half the leaf reflectance. In other words, the albedo of a stand of horizontal leaves, randomly distributed in space is one half the albedo of a monolayer of leaves. The albedo of a stand of strongly absorbing leaves is:

**Equation 9**

$$a_{canopy} = \frac{\rho_l}{2} (1 - \exp(-2L) + \alpha_{soil} \exp(-2L))$$

A graphical representation of this equation is shown.



A functional relationship between leaf area and albedo follow:

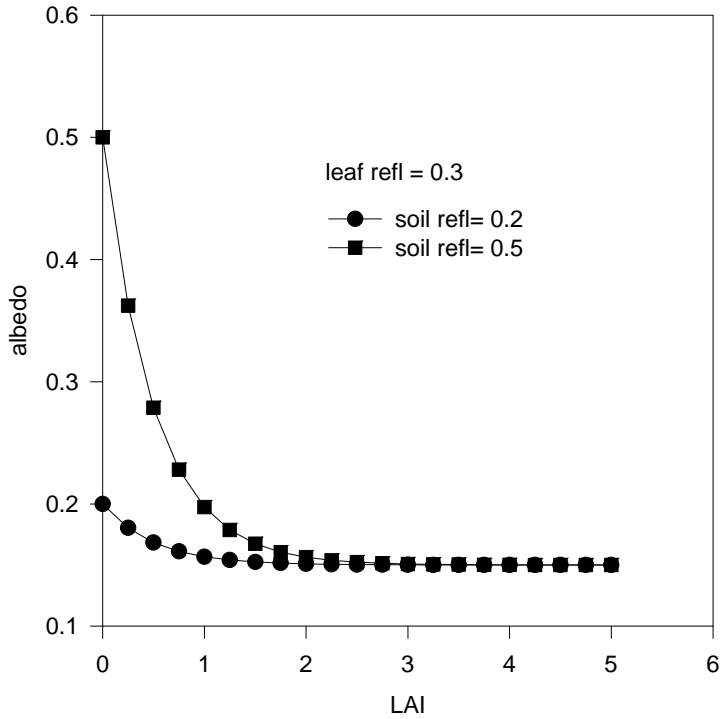


Figure 7 Albedo calculations as a function of leaf area index, using a simple big leaf model

Radiation reflected from a surface will depend on the origin and direction of light (direct or diffuse). Ross [Ross, 1980] weights albedo as a function of the direct and diffuse radiation and the reflectivities associated with those components.

**Equation 10**

$$\rho = \frac{\rho_{diffuse} + \rho_{direct} R_{beam} / R_{diffuse}}{1 + R_{beam} / R_{diffuse}}$$

Two types of scattering occur, isotropic and specular, which is equivalent to mirror reflection. In general, scattering is dependent upon the light wavelength, the direction of the source of light and the angular orientation of the leaf.

The impact of soil brightness is very important when LAI is below 2. As the canopy achieves closure, albedo is relatively independent of soil reflectivity, as there becomes a lower and lower probability that photons reflected by the soil will exit the canopy.

Model calculations of albedo for different wave bands and leaf angle distributions is listed below:

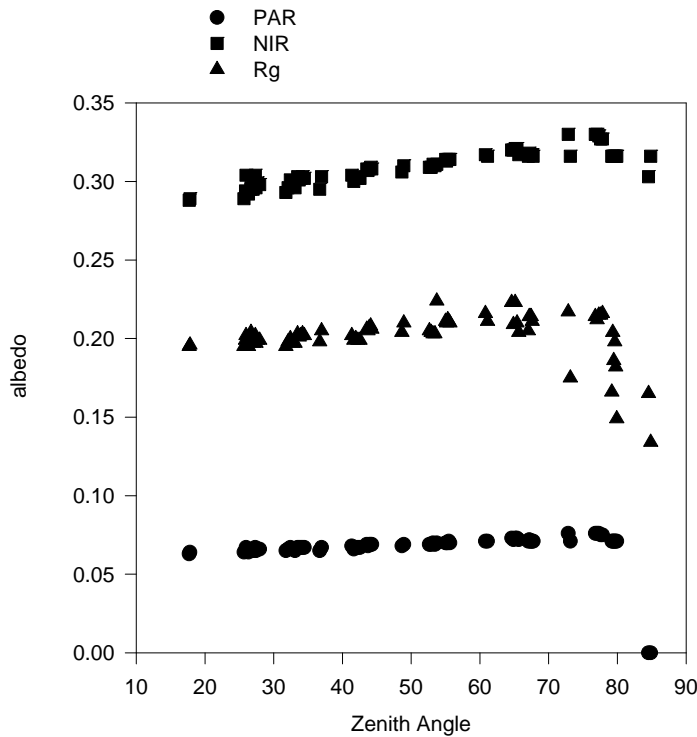


**Figure 8 Canopy reflectivity as a function of waveband and solar angle. These calculations were based on a slab layer model.**

With these calculations, albedo decreases as the sun approaches the horizon, as photons passing through the canopy must transcend through a longer distance. This effect leads to model predictions that show a reduction in albedo. This prediction is an oversimplification because directionally dependent scattering functions of leaves show higher reflectivity at low angles of incidence. More sophisticated models and field data show that albedo increases with increasing solar zenith.

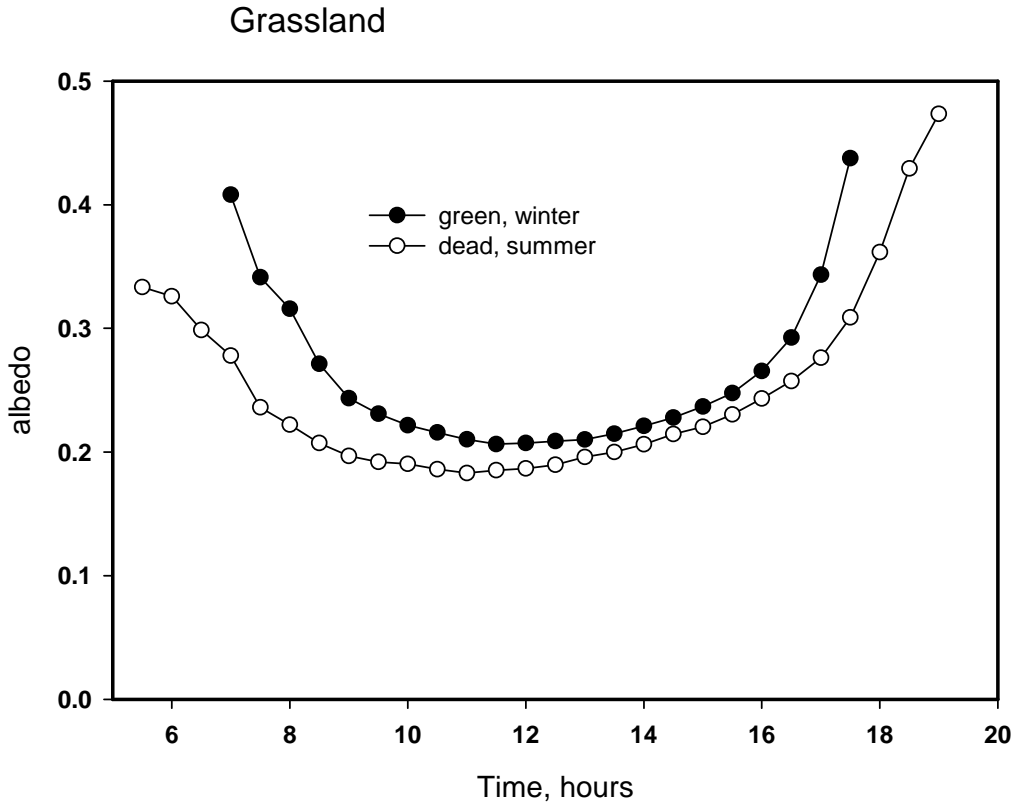


Figure 9 Diurnal pattern of albedo for two periods during the year over a California annual grassland.

Scientists are now able to measure albedo, globally and regularly with the MODIS satellite.

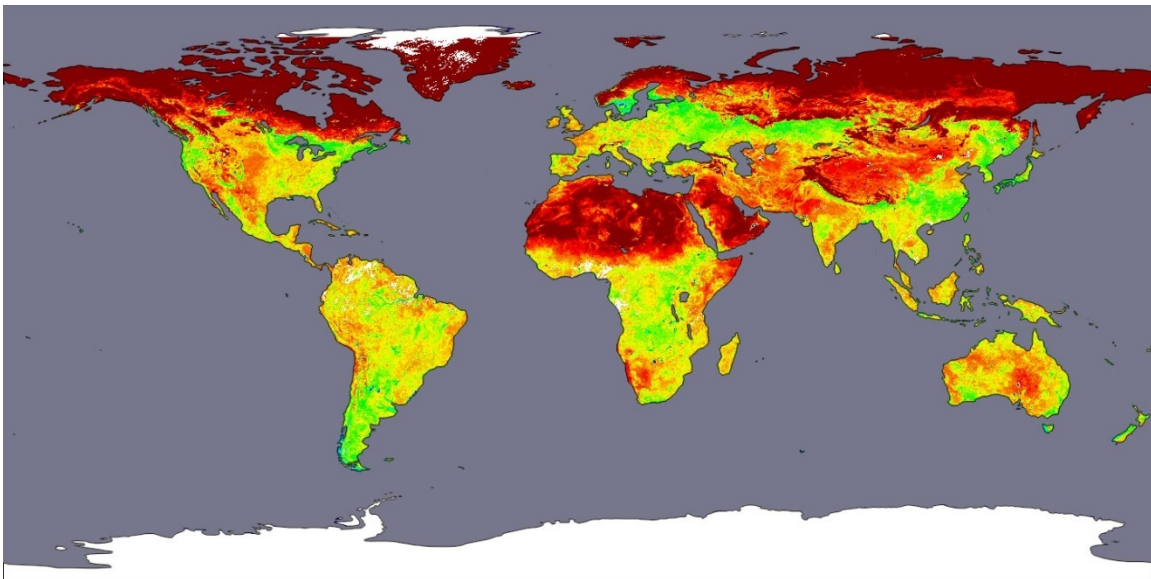


Figure 10 Modis Albedo. Boston University Dept of Geography, Remote Sensing Center

*Remote Sensing and Vegetation Indices (with assistance by Matthias Falk)*

The signal of electromagnetic radiation reflected or radiated by plants and soils is captured by satellites and used to interpret a broad array of canopy characteristics. The challenge and essence of remote sensing is to be able to interpret what radiation at various wavebands or narrow frequencies mean. Complication of interpretation is affected by the pixel size of the signal, the frequency on which the satellite repeats its visit and contamination by clouds, aerosols and gases.

A constellation of satellites is orbiting the Earth, each with a distinct use, history and technological capability. Table 3 is a listing of some of the main sensors used by biometeorologists and the colleagues and their key attributes. The Advanced Very High Resolution Radiometer (AVHRR) has the longest history. It is on a succession of NOAA satellites, with an original launch in 1979. It have been used to produce time series of the normalized difference vegetation index (NDVI), which in turn has been used to map LAI, phenology and land use change, as well as provide inputs into global inferred estimates of net primary productivity.

Landsat has high resolution than AVHRR, but a shorter record (Landsat 1, 1972 and Landsat 4 and 5 were launched in the 1980s). They have the thematic mapper with 6 reflectance and one thermal emittance band. Its pixel resolution is on the order of 30 m. Currently Landsat 7 is in operation. It repeats every 16 days and has 8 spectral bands in the visible, near infrared and thermal bands. Landsat 7 was launched in 1999 and is coming near the end of its 5 year life cycle. Politics may threaten the launching of a replacement. And recently LANDSAT data has been released to the general public, free.

**Table 2 Source, <http://homepage.mac.com/alexandreleroux/arsist/>; MODIS and Aviris web pages**

	resolution		repeat	duration
MODIS	250 m (bands 1-2) 500 m (bands 3-7) 1000 m (bands 8-36)	36 bands	1030 hrs Terra 1330 hrs Aqua (8 day composites are produced)	1999 Terra; 2002 Aqua
AVIRIS	20 m pixel, 11 km swath	224 contiguous spectral channels (bands) with wavelengths from 400 to 2500 nanometers, 10 nm.	Airborne on U2	On request
IKONOS	1m Panchromatic 4m multispectral (MS)	MS 4 bands (450-520, 520-600, 630-690, 760-900nm) Pan (525.8-928.5nm)	1-3 days	
SPOT-5	2.5 & 5m Pan	MS 4 bands (500-	3 to 26 days	

	10m MS 20m SWIR band	590, 610-680, 790-890, 1580-1750nm) Pan 510-730nm	$\pm 31^\circ$ inclination	
AVHRR	1 km pixel	4-5 broadbands (visible, NIR and thermal)	2399 km swath 14 times day, polar orbit	1978 to present
Landsat TM	15m Pan 30m MS 60m TIR I	Pan 520-900nm 5 Bands VNIR 2 Bands SWIR 1 Band TIR	16 days	1999 landsat 7

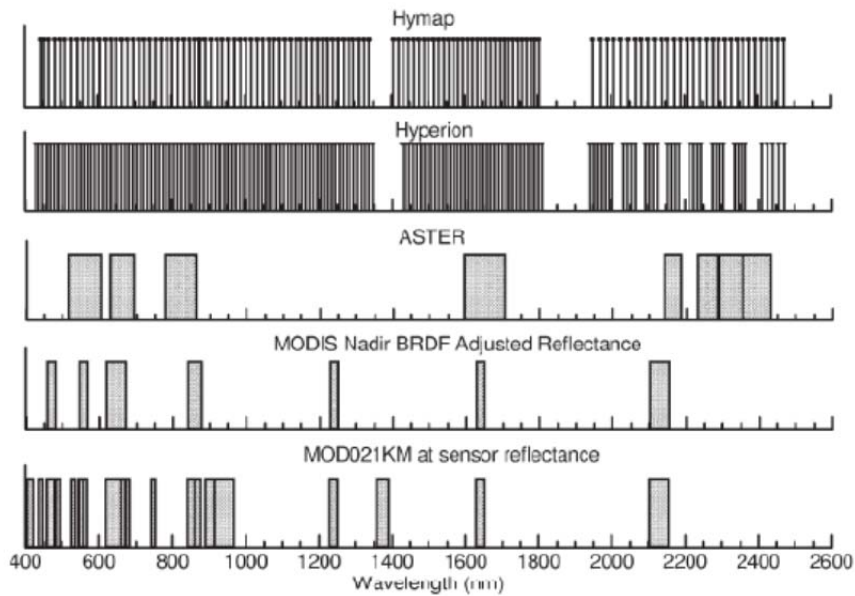


Figure 11 [Hill et al., 2006]

Hence the reflected solar spectrum can be viewed with a range of spectral resolution.

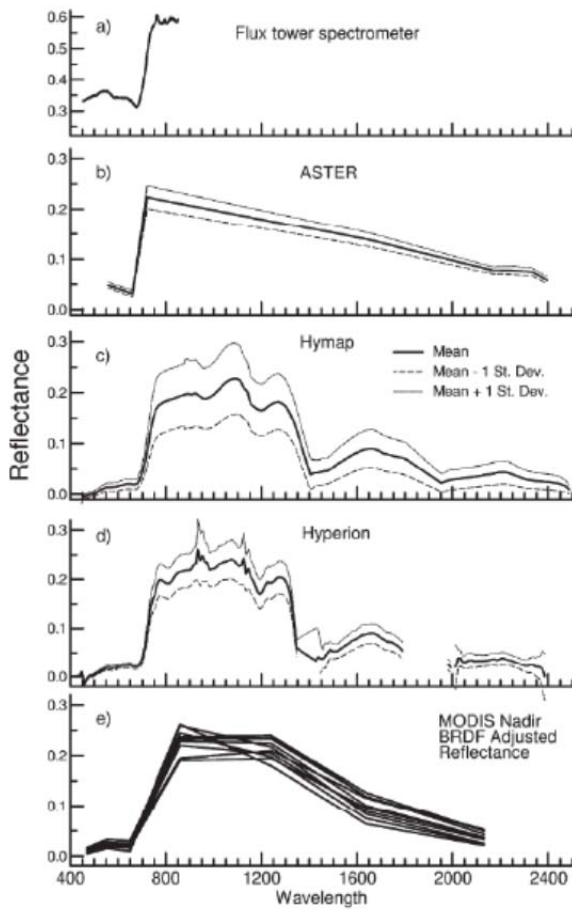
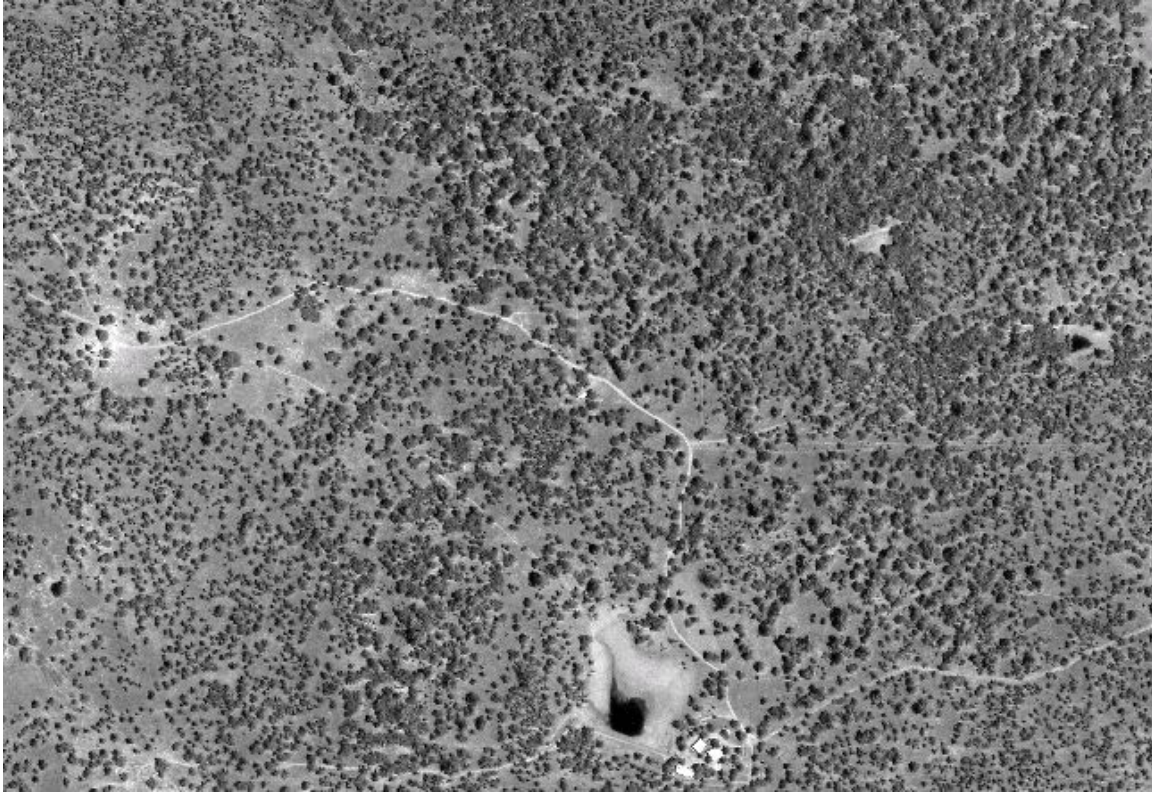


Figure 12 [Hill *et al.*, 2006]

IKONOS is a relatively new commercial sensor. It produces very high resolution information, but must be tasked, at a relatively high cost. The following picture is a panchromatic image of my oak savanna field site near Ione, CA. The image is about 1 km across and 1 m pixel resolution. It was taken by IKONOS. Note the detail of the trees, trails etc.



MODIS

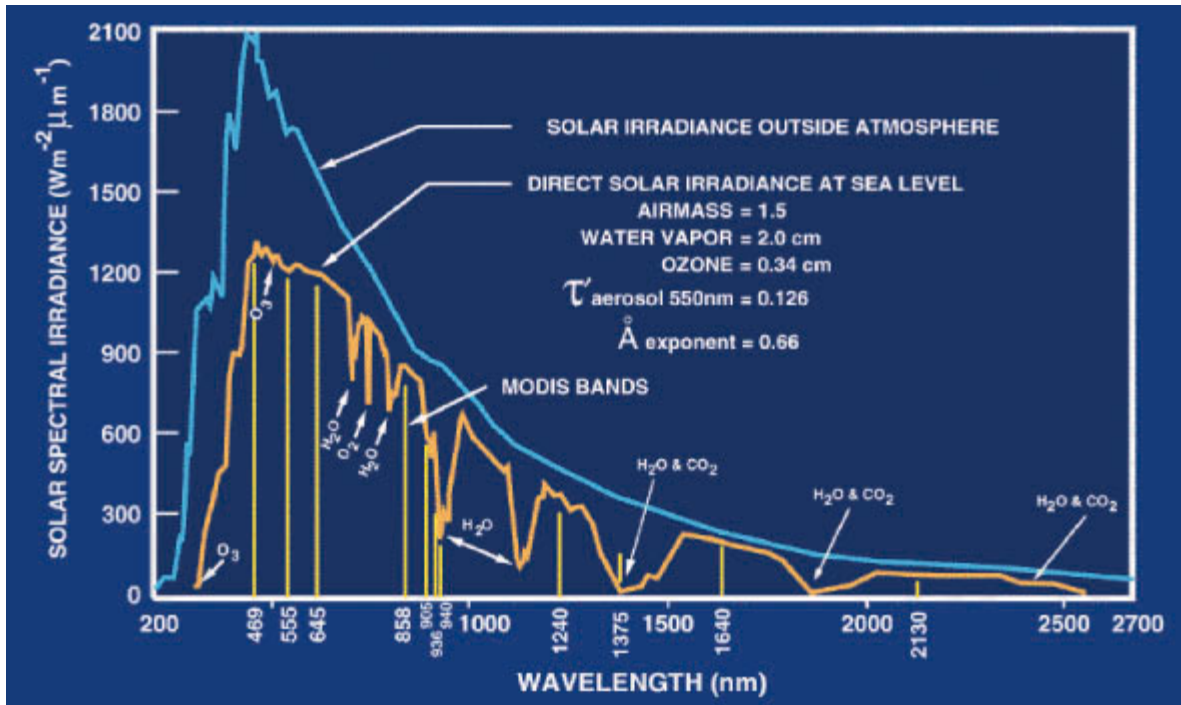


Figure 13 [http://upload.wikimedia.org/wikipedia/en/5/5e/MODIS\\_ATM\\_solar\\_irradiance.jpg](http://upload.wikimedia.org/wikipedia/en/5/5e/MODIS_ATM_solar_irradiance.jpg)

Table 4 is a brief survey of the various vegetation indices used by biometeorologists. Each has a different capability.

Table 3 Remote Sensing Indices

Normalized difference vegetation index	NDVI	$\frac{NIR - Red}{NIR + Red}$	
Enhanced vegetation index	EVI	$EVI = Gain \frac{NIR - Red}{C_1 + Red + (C_2 Red - C_3 Blue)}$	
Soil adjusted vegetation index	SAVI	$\frac{NIR - Red}{NIR + Red + L} (1 - L)$	
Photochemical reflectance index	PRI	$\frac{R_{531} - R_{570}}{R_{531} + R_{570}}$	
Simple ratio	SR	$\frac{NIR}{Red}$	

In general Simple Ratio (SR) does the best job of estimating the fraction of absorbed PAR (fpar). NDVI was originally interpreted as a measure of green leaf area biomass (Tucker 1979; 1980). Many studies have shown a strong relationship between NDVI and

LAI. One has to note though that NDVI tends to saturate with high. NDVI has a linear relationship with the fraction of incident photosynthetically active radiation (fPAR) absorbed by a canopy

The Enhanced Vegetation Index (EVI) was developed to offer an improvement over the NDVI by accounting for atmospheric contamination as well as soil background reflectance (Huete et al 1997, 2002; Justice et al. 1998). EVI normalizes the red band reflectance by the blue band reflectance (Huete et al 1997).

EVI is better correlated with high LAI where NDVI saturates quickly and shows very little dynamic range for high LAI canopies in crop fields (Boegh et al. 2002). EVI remains sensitive to variations of plant canopy (Huete et al. 2002). EVI is less sensitive than NDVI to residual atmospheric contamination such as aerosols from fires (Xiao et al 2003), however it is very problematic over snow and cloud cover ([http://tbrs.arizona.edu/project/MODIS/vi\\_quality.php](http://tbrs.arizona.edu/project/MODIS/vi_quality.php)). This problem results from use of the blue channel in the EVI for atmosphere resistance. It is generally assumed that for land surfaces  $\rho_{NIR} > \rho_{RED} > \rho_{BLUE}$  but this is not true for snow and cloud cover when  $\rho_{BLUE} > \rho_{RED} > \rho_{NIR}$ .

$$SAVI = (1+L) * (\rho_{NIR} - \rho_{RED}) / (L + \rho_{NIR} + \rho_{RED})$$

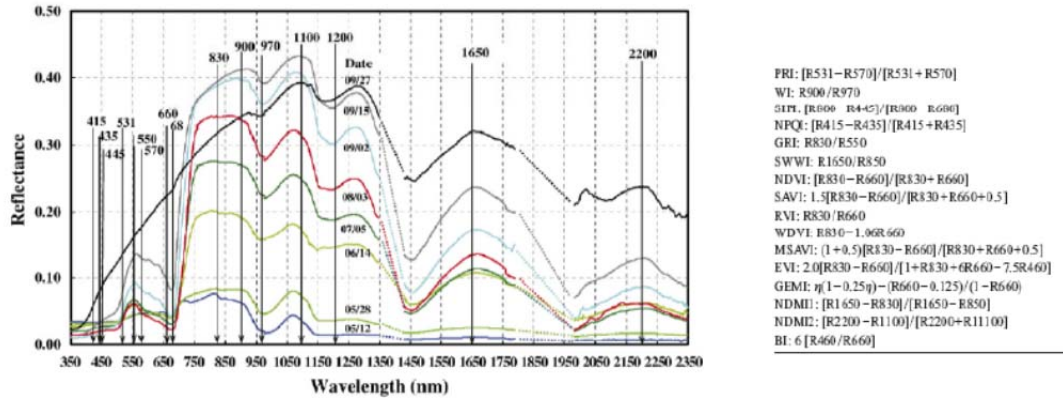
EVI is basically a modification of the SAVI with the addition of the **Blue** band for atmosphere resistance. In order to improve the EVI product over snow/cloud cover the algorithm simply turns off the atmosphere resistance component when there is snow and / or cloud - which means switching to the SAVI over the problem pixels (SAVI and EVI display an almost 1:1 relationship. The above three VIs are related to each other as follows:

$$\begin{aligned} NDVI & \text{====Soil Correction=====} > SAVI \\ NDVI & \text{====Atmosphere Adjustment=====} > ARVI \\ NDVI & \text{====Adjust for both=====} > EVI \end{aligned}$$

However for the broadband sensor setup used to calculate a tower based VI there is no practical way to calculate EVI or an EVI-like index since we are limited to 2 very broad bands. New sensors based on light emitting diodes might be able to provide tower sites with a economic way to add further bands in the visible spectrum. One also has to note that for tower mounted instrumentation the relative contamination of measured reflected radiation to aerosol contamination has to be small.

Electromagnetic radiation used by the PSII photosynthetic pathway is either used to produce photochemical energy or it is dissipated to reduce damage of pigments. PRI was developed by Gamon and colleagues [*Gamon et al.*, 1992; *Gamon et al.*, 1997]. It's strength is in detecting stress on photosynthesis due to the fluorescent emission of energy. IT is a measure of the efficiency of PSII.

In recent years, with the availability of high resolution spectral reflectance measurements investigators are examining a wider range of indices for predicting CO<sub>2</sub> exchange [*Inoue et al.*, 2008; *Rahman et al.*, 2004; *Rahman et al.*, 2005].



Inoue et al 2008. RSE

## References

- Gates, D.M., H.J. Keegen, J.C. Schleiter and V.R. Weidner. 1965. Spectral properties of plants. *Applied Optics*. 4: 11-20.
- Myneni, RB, Asrar, G, Kanemasu, ET. 1989. The theory of photon transport in leaf canopies. In: *Theory and Application of Optical Remote Sensing*. Ed. Asrar. John Wiley
- Ross, J. 1975. Radiative Transfer in Plant Communities, In: *Vegetation and the Atmosphere*, I. J.L. Ross (ed). Academic Press. pp 13-55.
- Tang, Y. Light. In: *Plant Ecophysiology*. Ed MNV Prasad. John Wiley. New York. Pp 3-40.

## APPENDIX

**Table 4 General properties of MODIS**

	Bands	Range (start)
Land/cloud/aerosols boundary	1,2	620; 841 nm
Land/cloud/aerosols properties	3-7	459; 545; 1230; 1628; 2105
Ocean color/ phytoplankton	8-16	405;438; 483;526;546;622;673;743;862
Atmospheric vapor	17-19	890; 931;913
Surface/cloud temperature	20-23	3666;3929;4020
Atmospheric temperature	24-25	4433;4482
Cirrus cloud vapor	26-28	1360;6535;7175
Cloud prop	29	8400
ozone	30	9580
Surface/cloud temperature	31-32	10780;11770
Cloud top altitude	33-36	13185;13485;13785;14085

**Table 5 Details of AVHRR**

AVHRR Spectral Ranges				
Band Number	NOAA Satellites: 6, 8, 10	NOAA Satellites: 7, 9, 11,12,14	NOAA Satellites: 15, 16, 17	IFOV
1	0.58 - 0.68	0.58 - 0.68	0.58 - 0.68	1.39
2	0.725 - 1.10	0.725 - 1.10	0.725 - 1.10	1.41
3 (A)			1.58 - 1.64	1.30
3 (B)	3.55 - 3.93	3.55 - 3.93	3.55 - 3.93	1.51
4	10.50 - 11.50	10.30 - 11.30	10.30 - 11.30	1.41
5	band 4 repeated	11.50 - 12.50	11.50 - 12.50	1.30
	(in micrometers)	(in micrometers)	(in micrometers)	(in milliradians)

**Table 6 Spectral Band Characteristics (grey bands used for NDVI)**

Compiled by Matthias Falk

Band/Sensor	NOAA- AVHRR	Landsat TM	MODIS	IKONOS	Flux To
Blue		0.45-0.52 $\mu\text{m}$	0.459-0.479 $\mu\text{m}$	0.455-0.516 $\mu\text{m}$	
Green	0.55-0.68 $\mu\text{m}$	0.53-0.60 $\mu\text{m}$	0.545-0.565 $\mu\text{m}$	0.506-0.595 $\mu\text{m}$	0.40-0.7

Red		0.63-0.69 $\mu\text{m}$	0.620-0.670 $\mu\text{m}$	0.632-0.698 $\mu\text{m}$	
NIR	0.735-1.1 $\mu\text{m}$	0.76-0.90 $\mu\text{m}$	0.841-0.876 $\mu\text{m}$	0.757-0.853 $\mu\text{m}$	0.70-1.1
Middle-IR			1.230-1.250 $\mu\text{m}$		
Middle-IR		1.55-1.75 $\mu\text{m}$	1.628-1.652 $\mu\text{m}$		
Middle-IR		2.08-2.35 $\mu\text{m}$	2.105-2.155 $\mu\text{m}$		
Pixel size at nadir	1 km	30 m	1.0 km	1 m	$\sim 100 \text{ m}^2$
Temporal	Daily	16 days	16 days	snapshot	30 min

## ENDNOTES

- Dickinson, R.E., Land surface processes and climate-surface albedos and energy balance, *Advances in Geophysics*, 25, 305-353, 1983.
- Gamon, J.A., J. Penueles, and C.B. Field, A narrow-waveband spectral index that tracks diurnal changes in photosynthetic efficiency, *Remote Sensing of Environment*, 41 (1), 35-44, 1992.
- Gamon, J.A., L. Serrano, and J.S. Surfus, The photochemical reflectance index: an optical indicator of photosynthetic radiation use efficiency across species, functional types, and nutrient levels, *Oecologia*, 112 (4), 492-501, 1997.
- Gates, D.M., *Biophysical Ecology*, 611 pp., Dover, Mineola, NY, 1980.
- Gates, D.M., H.J. Keegan, J.C. Schleter, and V.R. Weidner, Spectral Properties of Plants, *Applied Optics*, 4 (1), 11-&, 1965.
- Hill, M.J., A.A. Held, R. Leuning, N.C. Coops, D. Hughes, and H.A. Cleugh, MODIS spectral signals at a flux tower site: Relationships with high-resolution data, and CO<sub>2</sub> flux and light use efficiency measurements, *Remote Sensing of Environment*, 103 (3), 351-368, 2006.
- Inoue, Y., J. Penueles, A. Miyata, and M. Mano, Normalized difference spectral indices for estimating photosynthetic efficiency and capacity at a canopy scale derived from hyperspectral and CO<sub>2</sub> flux measurements in rice, *Remote Sensing of Environment*, 112 (1), 156-172, 2008.
- Kubelka, P., New Contributions to the Optics of Intensely Light-Scattering Materials .1, *Journal of the Optical Society of America*, 38 (5), 448-457, 1948.
- Kubelka, P., and F. Munk, An article on the optics of paint layers, *Z. Tech Physik*, 1931.
- Myneni, R.B., J. Ross, and G. Asrar, A review on the theory of photon transport in leaf canopies, *Agricultural and Forest Meteorology*, 45 (1-2), 1-153, 1989.
- Norman, J.M., Modeling the complete crop canopy., in *Modification of the aerial environment of plants*, edited by B.J. Barfield and J.F. Gerber, pp. 249-277, , American Society of Agricultural Engineering, St. Joseph, MI, 1979.
- Norman, J.M., and P.G. Jarvis, Photosynthesis in Sitka Spruce (*Picea-Sitchensis* (Bong) Carr) .5. Radiation Penetration Theory and a Test Case, *Journal of Applied Ecology*, 12 (3), 839-878, 1975.
- Norman, J.M., E.E. Miller, and C.B. Tanner, Light Intensity and Sunfleck-Size Distributions in Plant Canopies, *Agronomy Journal*, 63 (5), 743-&, 1971.

- Rahman, A., V. Cordova, J. Gamon, H. Schmid, and D. Sims, Potential of MODIS ocean bands for estimating CO<sub>2</sub> flux from terrestrial vegetation: A novel approach, *Geophysical Research Letters*, 31, doi:10.1029/2004GL019778, 2004.
- Rahman, A.F., D.A. Sims, V.D. Cordova, and B.Z. El-Masri, Potential of MODIS EVI and surface temperature for directly estimating per-pixel ecosystem C fluxes, *Geophysical Research Letters*, 32 (19), 2005.
- Ross, J., *The Radiation Regime and Architecture of Plant Stands.*, Dr. W Junk, The Hague, 1980.
- Suits, G.H., The calculation of the directional reflectance of a vegetative canopy, *Remote Sensing of Environment*, 2, 117-125, 1971.